Supporting Information

Virus-directed formation of electrocatalytically active nanoparticle-based Co_3O_4 tubes

Anna S. Schenk,[,a] Sabine Eiben,[b] Miriam Goll,[a] Lukas Reith,[a] Alex N. Kulak,[c] Fiona C. Meldrum,[c]*

Holger Jeske,[b] Christina Wege,[b] and Sabine Ludwigs[,a]*

[a] Institute of Polymer Chemistry, University of Stuttgart, Pfaffenwaldring 55, 70569 Stuttgart, Germany

[b] Institute of Biomaterials and Biomolecular Systems, University of Stuttgart, Pfaffenwaldring 57, 70569 Stuttgart, Germany

[c] School of Chemistry, University of Leeds, Woodhouse Lane, LS2 9JT Leeds, United Kingdom

**E-Mail: anna.schenk@ipoc.uni-stuttgart.de; sabine.ludwigs@ipoc.uni-stuttgart.de*

Contents

1. Materials and Methods

1.1 Chemicals.

All reactant solutions were prepared using deionized water (ELGA Maxima, resistivity = 18.2 MΩcm). Commercially available reagents were purchased in analytical grade and applied without further purification. Cobalt(II) chloride hexahydrate ($CoCl_2 \cdot 6H_2O$) and ammonium carbonate ($(NH_4)_2CO_3$) reagents as well as ethanol absolute were purchased from Sigma Aldrich. Wild-type tobacco mosaic viruses (TMV) were isolated and purified according to the procedures detailed below. Glassy carbon particles (spherical powder, 2-12 µm) and Nafion perfluorinated resin solution (5 wt% in lower aliphatic alcohols and water, 15-20 % water) for the preparation of electrodes for oxygen electrocatalysis as well as a cobalt(II,III) oxide (nanopowder < 50 nm particle size) for reference purposes were purchased from Sigma Aldrich. Sodium hydroxide was obtained from ABCR GmbH.

1.2 Isolation and Purification of Tobacco Mosaic Virus Particles.

Tobacco mosaic virus strain U1 was propagated in Nicotiana tabacum 'Samsun' nn plants for 4 weeks following mechanical inoculation. Virus particles were isolated from freshly harvested or frozen leaves according to a modified protocol of Chapman.[1] The virus particles were either stored in 10 mM sodium potassium phosphate (SPP) buffer, pH 7.4 or in dd H_2O at a standard concentration of 10 $g \cdot L^{-1}$ at 4 °C until further use.

1.3 Investigation of the Aggregation Behavior of TMV in $CoCl_2$-solution.

Dynamic Light Scattering (DLS). DLS measurements on TMV/ $CoCl_2$ mixtures with different Co(II) concentrations were performed using the Malvern Nanosizer ZS (Malvern Instruments, Worcestershire, UK). For size measurement BRAND® UV cuvettes micro were filled with a sample volume of 100 µl. Data were obtained by applying automatic measurement duration, positioning and attenuator settings in the backscattering mode at 173°. Z-average was used as a measure for the size of the aggregates present in the reaction mixture. Due to the rod-like structure of TMV the hydrodynamic radius, calculated for spheres, is shown as apparent hydrodynamic radius. The polydispersity index was between 0.1 and 0.31 for all samples. Folded capillary zeta cells (Malvern Instruments, Worcestershire, UK) were used for zeta potential determination. Three measurements with automatic subruns were performed for each TMV/ $CoCl_2$ mixture. The zeta potential was evaluated according to the Smoluchowski equation. The same mixtures of TMV and $CoCl_2$ were used for both measurement modes, size and zeta potential. For each sample 500 µl TMV 0.2 $g \cdot L^{-1}$ in H_2O were mixed with 500 µl of dd

H_2O or either 0.2, 2, 20 or 200 mM $CoCl_2$, incubated for 30 min and then centrifuged 5 min at 5,000 g at room temperature in a tabletop centrifuge (Eppendorf, Hamburg, Germany). Size measurements were performed with 100 µl of the supernatant, while 800 µl were used for determination of the zeta potential. TMV in 10 mM SPP pH 7.4 at 0.1 $g \cdot L^{-1}$ was analyzed for reference.

TEM and Sample Preparation/ Staining. For the preparation of TEM samples the pellet of a 0.1 $g \cdot L^{-1}$ TMV and 100 mM $CoCl_2$ solution obtained after centrifugation at 5,000 g for 5 min was re-suspended in 100 µl dd H_2O. For comparison the supernatant of a 0.1 $g \cdot L^{-1}$ solution of TMV in 10 mM SPP pH 7.4 after centrifugation at 20,000 g for 5 min was used. The TMV solutions were adsorbed on Formvar®-coated, carbon-sputtered 400 mesh copper grids (Ted Pella, Redding, CA) for 10 min followed by washing of each grid 3 times with dd H_2O for 30 seconds and staining with 2 % uranylacetate by placing the grids on three droplets of uranyl acetate for 2 x 30 seconds and once 90 seconds. After removal of excess solution with filter paper the grids were investigated on a Tecnai G2 Sphera FEI TEM (FEI, Eindhoven, Netherlands) at 120 kV. TEM images were recorded by a 16 megapixel camera (TemCam-F416 [4k × 4k], TVIPS, Gauting, Germany).

1.4 Precipitation of Basic Cobalt Carbonate and Transformation into Cobalt(II,III) Oxide.

Basic cobalt carbonate was precipitated from aqueous solutions of cobalt(II) chloride hexahydrate ($[CoCl_2 \cdot 6H_2O]$ = 100 mM) using the ammonium carbonate diffusion technique. In this reaction setup, glass vials containing 10 mL of the Co(II) solution were covered with Parafilm, which was subsequently punched with 5 needle holes. These vials were then placed in a sealed desiccator together with two more vials of the same size, each filled with 5 g of ammonium carbonate and also covered with Parafilm, into which 5 needle holes were punched. Typically, the Co(II)-solutions were exposed to the CO_2 and NH_3 vapor phase formed by decomposition of the solid $(NH_4)_2CO_3$ for 2 days. In order to study the evolution of particle morphologies and composition, samples were also drawn after shorter periods of time (12 hours, 24 hours, 36 hours). The obtained products were then filtered under vacuum and the solid residues were rinsed with copious amounts of deionized water and ethanol. After drying, the solids were stored in a desiccator under vacuum. In order to convert the basic cobalt carbonate precursor into spinel-type cobalt oxide, the samples were annealed in a tube furnace at 400°C under air atmosphere for 2 hours.

Mineral Precipitation in the Presence of Tobacco Mosaic Viruses. To evaluate the structure-directing effects of virus particles on the formation of the mineral phase, samples were prepared as described above, but with different amounts of TMV ($[CoCl_2 \cdot 6H_2O]$ = 100 mM,

[TMV] = 0.02 $g \cdot L^{-1}$, 0.1 $g \cdot L^{-1}$ or 0.5 $g \cdot L^{-1}$) added to the cobalt solution before exposure to ammonium carbonate vapor.

Ammonium Carbonate Diffusion Experiments with Cobalt-Free Virus Suspensions. As a control experiment, we studied whether precipitation of the virus particles can be induced during the ammonium carbonate diffusion reaction in the absence of Co(II)-ions due to the change in pH and a concomitant formation of carbonate ions. For this purpose, TMV dispersions were prepared in ultra-pure water at the same concentrations as typically used in our mineralization experiments. Reaction vials containing 10 mL of these solutions were then placed in a desiccator and exposed to ammonium carbonate vapor for 2 days. Under these conditions the solution stayed clear and we did not observe any indication for phase separation or aggregate formation in the absence of Co(II)-ions. Hence, the virus particles do not seem to be sensitive to pH changes in the range relevant for our mineralization experiments nor to the presence of corresponding amounts of carbonate ions.

1.5 Structural Characterization of the Precipitates.

Light Microscopy. Information on the overall morphology of the samples was obtained by light microscopy and polarized optical microscopy (POM) performed in the reflected light mode with an Axio Imager.A1 microscope from Zeiss.

Scanning Electron Microscopy (SEM). Scanning electron micrographs were recorded using a Hitachi S-4800 instrument operated in the deceleration mode with landing voltages of 0.5 or 1 kV. Powder specimens were typically prepared for imaging by dispersing a small amount of the material in ethanol and pipetting a droplet of this suspension onto a fragment of a silicon wafer. After evaporation of the solvent, these shards were then fixed on SEM stubs with the help of adhesive carbon tapes. All samples were investigated in their pristine state without an additional conductive coating.

Transmission Electron Microscopy (TEM). TEM and selected area electron diffraction (SAED) of precursor precipitates as well as cobalt(II,III) oxide samples obtained after calcination were performed on a Phillips CM-200 FEG-TEM operating at 200 kV. Samples containing microparticles were slightly ground with a mortar and pistil. The resulting powders were then dispersed in ethanol and a small droplet of these suspensions was pipetted onto copper TEM grids coated with a film of Formvar® and carbon. The samples were dried under vacuum before being transferred to the electron microscope.

Vibrational Spectroscopy. An IFS 66/S FT-IR spectrometer from Bruker was used to record infra-red spectra of powdered samples in a wavelength range from 700-3500 cm^{-1}. The instrument was equipped with a diamond ATR (golden gate) unit purchased from Specac.

Selected samples were also investigated by Raman spectroscopy using an inVia-Raman microscope equipped with a 785 nm diode laser (Renishaw Raman 2000). In this case, the laser was focused onto individual particles through a 50x objective (numerical aperture NA 0.75) and the laser power was adjusted such that sample degradation was prevented.

Thermal Analysis. Simultaneous thermogravimetric analysis (TGA) and differential scanning calorimetry (DSC) were performed to analyze the composition of the mineral precursor phase and the temperature range in which transformation into cobalt(II,III) oxide occurs. The measurements were carried out with an STA 449C instrument (NETZSCH, Germany). Data were recorded under synthetic air atmosphere (100 $mL \cdot min^{-1}$) in a temperature range between 25°C and 600°C with a heating rate of 10°C·min^{-1}. Additionally, a concentrated suspension of TMV in water was analyzed for reference. In order to allow complete evaporation of excess water to resolve the decomposition of the protein-based virus particles, this non-mineralized sample was subjected to a heating regime including the following steps: (1) heating from 20°C to 100°C at 10°C·min^{-1}, (2) keeping the sample at a temperature of 100°C for 1 min, and (3) heating from 100°C to 600°C at 10°C·min^{-1}.

Powder X-Ray Diffraction (PXRD). X-ray diffraction of finely ground powders was carried out for phase identification. All measurements were performed in Bragg-Brentano geometry on a Rigaku SmartLab instrument using monochromatic Cu-Kα radiation at 40 kV and 40 mA. Data were recorded in an angular range between 10° and 90° in steps of 0.04° with a scan rate of 0.5°·min^{-1}.

SDS-Polyacrylamide Electrophoresis and Western Blot Analysis. To investigate the presence of TMV in the basic cobalt carbonate superstructures, 5 mg of the material were finely ground and heated for 10 min in 50 µl 2x Laemmli sample buffer. After addition of 50 µl dd H_2O the samples were centrifuged for 1 min at 20,000 g and 8 µl loaded on a 15 % discontinuous, denaturing polyacrylamide gel. PageRuler™ (Thermo Fischer Scientific, Waltham, USA) and 250 ng of pure TMV were applied as standards. The gel was run at 25 mA for 90 minutes and then blotted onto a nitrocellulose membrane (Protran®, Whatman, Dassel, Germany) by semi-dry blotting. As primary antibody α-TMV (kindly provided by Prof. K.W. Mundry) to detect TMV CP in the material, followed by secondary alkaline phosphatase-coupled α-rabbit antibody (Rockland Immunochemicals, Gilbertsville, USA) were used and visualized using nitro blue tetrazolium chloride/5-bromo-4-chloro-3-indolyl phosphate (NBT/BCIP) as substrate.[2]

Nitrogen Adsorption (BET). Surface area analysis according to the Brunauer-Emmett-Teller (BET) theory was conducted based on N_2 adsorption isotherms obtained with a Micrometrics ASAP 2020 instrument after degassing the sample for 3h at 120°C. The specific surface area

was calculated from the linear part of the BET plot. For each specimen 5 data points of P/P_0 were measured using ≈100 mg of material.

1.6 Functional Properties in Oxygen Electrocatalysis.

In order to determine and compare the electrocatalytic activity of the different cobalt oxide materials towards the oxygen evolution reaction (OER), the powders were immobilized on glassy carbon working electrodes. For this purpose, suspensions of the Co_3O_4 particles were prepared in a water/ alcohol mixture together with Nafion as binder and glassy carbon powder as conductive support. These suspensions were homogenized by ultrasonification and then drop-casted on a polished glassy carbon rotating disc electrode (GC-RDE) with a diameter of 3 mm. The electrodes were then blown dry with argon. Typically, this procedure resulted in a loading of 0.25 $mg \cdot cm^{-2}$ cobalt oxide powder, 0.05 $mg \cdot cm^{-2}$ glassy carbon powder and 0.05 $mg \cdot cm^{-2}$ Nafion. Alternatively, electrodes were prepared with higher loading (1.4 $mg \cdot cm^{-2}$ of cobalt oxide powder, 2.2 $mg \cdot cm^{-2}$ of glassy carbon powder and 0.6 $mg \cdot cm^{-2}$ of Nafion). Scanning electron micrographs were recorded to confirm a homogeneous distribution of the cobalt oxide particles in the mixture. Samples for SEM imaging were prepared from the same suspensions as used for electrochemical testing directly on conducting substrates.

All electrochemical experiments were performed with an Autolab PGSTAT101 potentiostat in a three-electrode glass cell in 0.1 M NaOH in ultrapure water (18.2 MΩcm) under inert gas atmosphere at room temperature. A glassy carbon rod was used as counter electrode and the reference was a double junction Ag/AgCl (3M KCl) electrode with a ground-joint diaphragm. The rotation speed of the rotating disc electrode (RDE) was set to 2,000 r.p.m. for all OER measurements. The uncompensated solution resistance R_u was determined using the current-interrupt method (a typical value was 80 Ω). The measured potentials were converted to the reversible hydrogen electrode (RHE) scale and corrected for the iR-drop according to the equation $E_{RHE} = E_{Ag/AgCl} + 0.059 \cdot pH + E^0_{Ag/AgCl}(3M\ KCl) - iR_u$, where E_{RHE} is the converted potential, $E_{Ag/AgCl}$ is the measured potential vs the here used Ag/AgCl electrode, $E^0_{Ag/AgCl\ (3M\ KCl)}$ equals 0.205 V[3] and i represents the measured current. Overpotentials for the OER are given as $\eta = E_{RHE} - E_{H2O/O2}$, where $E_{H2O/O2}$ is the standard potential of the OER vs RHE, 1.229 V. Current densities are calculated using the geometric surface area. For each material at least 10 electrodes were prepared and the average values for the overpotentials determined from these measurements are presented together with standard deviations.

2. Supplementary Figures and Legends

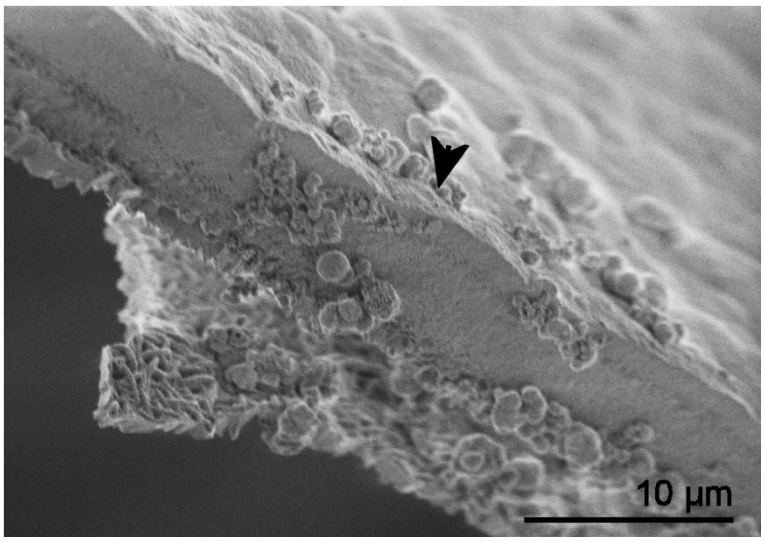

Figure S1. Cross section of a mineral sheet formed at the air/ solution interface under additive-free conditions imaged by scanning electron microscopy. The arrow head points to the air-exposed side of the film, where the material appears to be denser. On the opposite side, nucleation of platelet-shaped particles facing towards the solution is frequently seen.

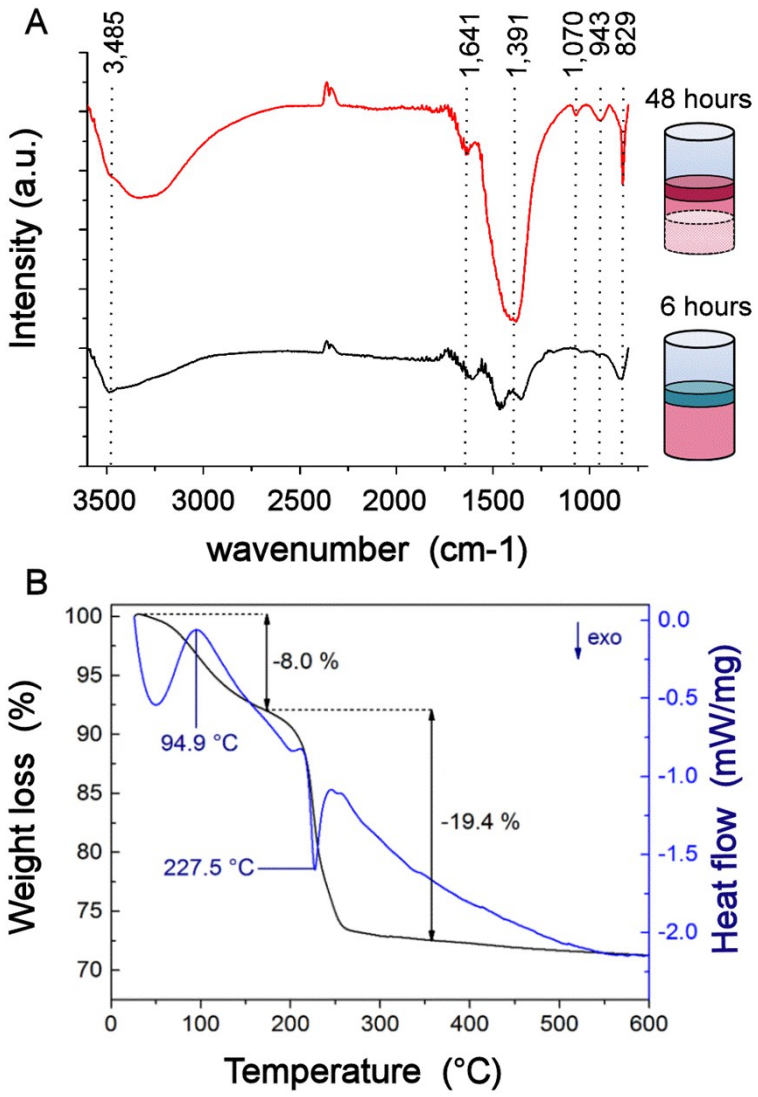

Figure S2. Chemical composition of a mineral precursor sample precipitated from a 100 mM solution of Co(II) by ammonium carbonate diffusion. A) Infra-red spectra recorded after 6 hours (black line) and 48 hours (red line) of reaction time are shown. The schematics on the right illustrate the composition of the sample at both time points. While only a blue-greenish film-like material is formed at the air/ solution interface after 6 hours, the sample obtained after 48 hours is constituted from a more solid, dark pink interface-grown film accompanied by a major phase of light pink bulk precipitate. B) Thermal analysis of the mature precipitate extracted after 48 hours. TGA (black line) and DSC (blue line) curves are presented.

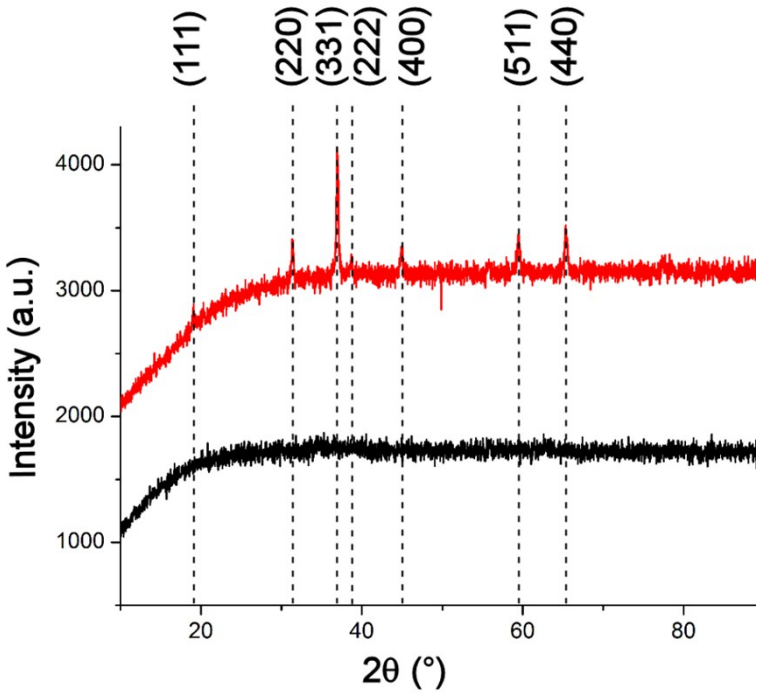

Figure S3. Powder x-ray diffractogram of mineral precipitated from a 100 mM Co(II)-solution under additive-free conditions. Diffraction data were recorded before (black curve) and after calcination (red curve). Peaks in the diffractogram of the calcined sample can be assigned to spinel-type cobalt oxide. A strong background attributable to x-ray fluorescence is seen in both curves.

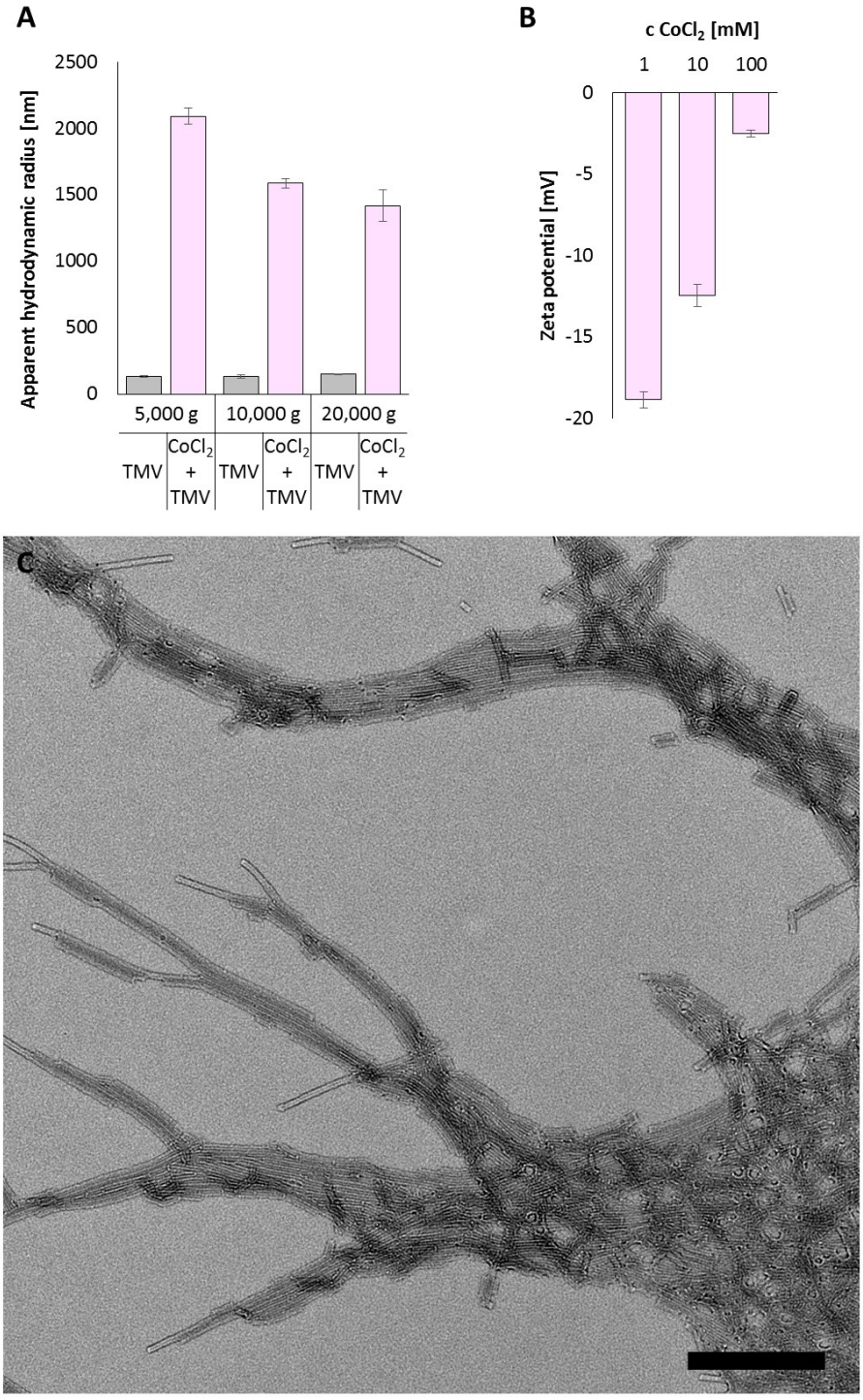

Figure S4. Properties of TMV in $CoCl_2$ solutions. A) Hydrodynamic radii of TMV/ $[Co^{2+}]$ aggregates present in the supernatant of solutions with [TMV]= 0.1 g·L^{-1} and Co^{2+} concentrations of $[Co^{2+}]$ = 0 mM, (grey bars) or $[Co^{2+}]$ = 100 mM (pink bars) after centrifugation at 5,000 g, 10,000 g and 20,000 g. B) zeta potential of TMV, 0.1 g·L^{-1}, depending on the $[Co^{2+}]$ concentration. C) The TEM image represents an enlarged view of Fig. 3C showing the aggregation of TEM in the presence of Co(II)-ions ($[Co^{2+}]$ = 100 mM). The dark edges are due to staining with uranyl acetate to increase the contrast of the protein-based particles. Scale bar = 300 nm.

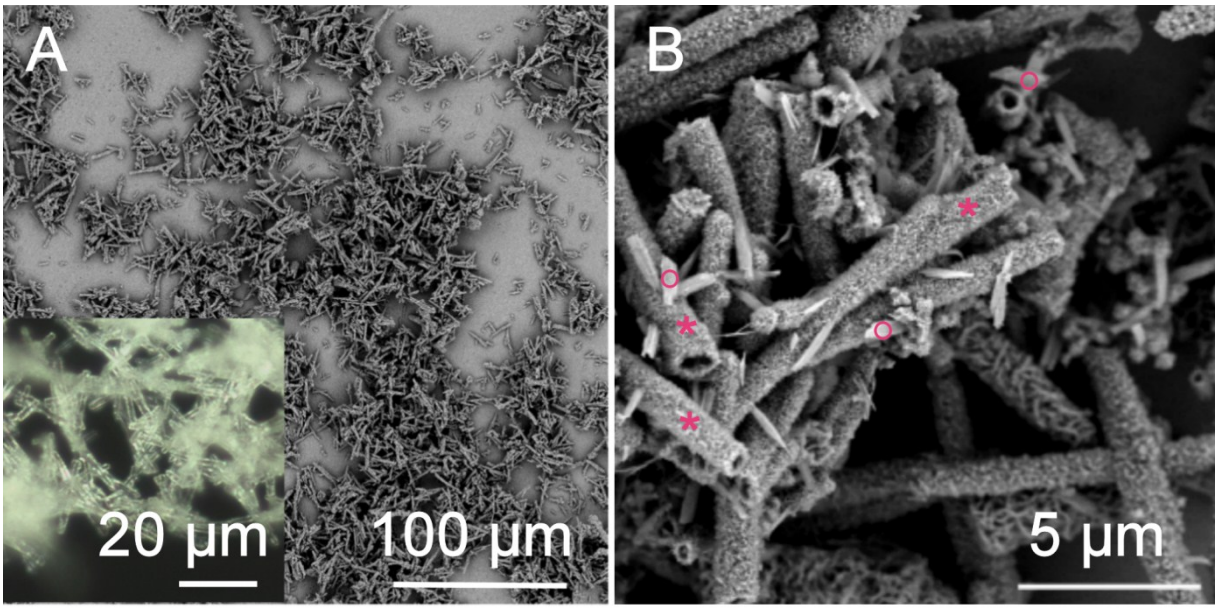

Figure S5. Morphology of basic cobalt carbonate precipitated from a 100 mM Co^{2+} solution in the presence of tobacco mosaic viruses (wild type, [TMV] = 0.1 g·L^{-1}). A) Scanning electron micrograph showing micrometer-sized mineralized rods. Polarized light microscopy (inset) reveals a crystalline nature of the cylindrical particles. B) At higher magnifications a rough-textured surface topography is visible. Some of the rods appear hollow with channel diameters in the range of 0.5 – 2 µm. The rods and tubules (*) are accompanied by a minor fraction of small mineral flakes (o).

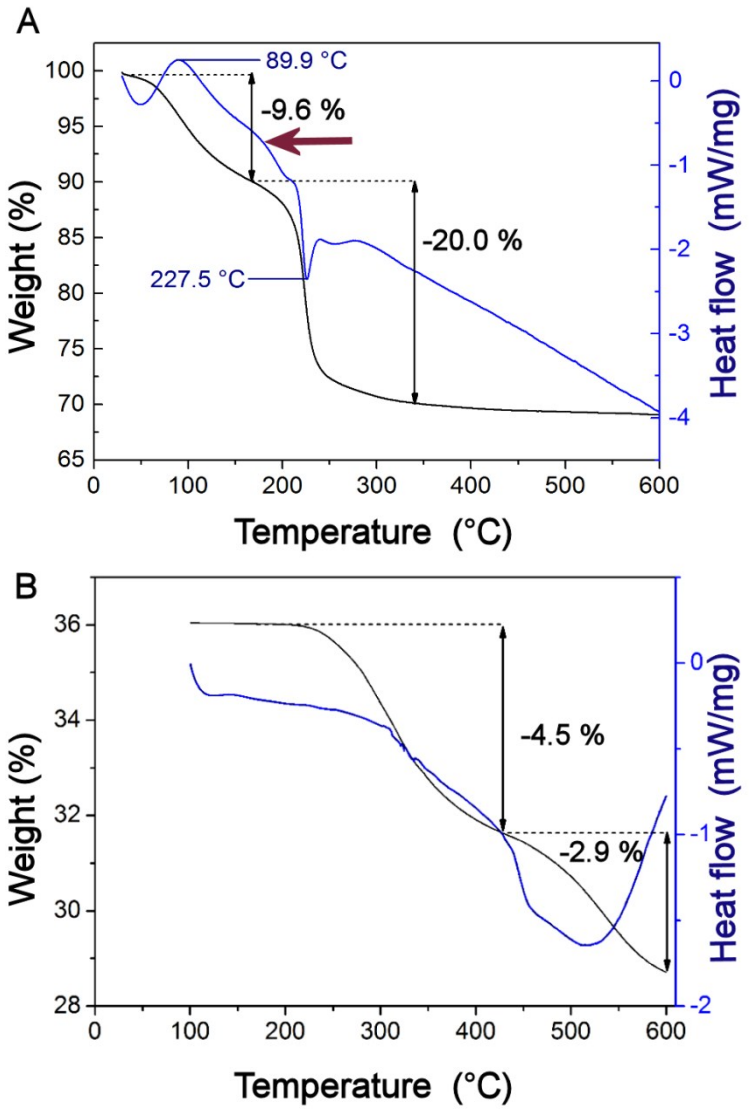

Figure S6. Thermal analysis of TMV/ mineral composite particles (A) and non-mineralized TMV particles in buffer solution (B). TGA (black) and DSC (blue) curves are presented. The small shoulder in the DSC profile of the composite (marked by red arrow in (A)) does not appear to coincide with any thermal events in the virus sample (B).

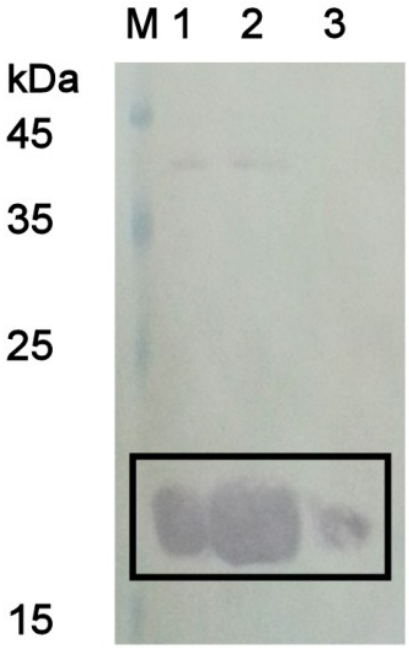

Figure S7: Western blot analysis with TMV-specific antibodies confirms the presence of virus coat protein in mineral samples prepared with 0.1 g·L^{-1} (1) and 0.5 g·L^{-1} (2) concentrations of TMV. For comparison, a sample of 250 ng pure TMV coat protein is shown (3).

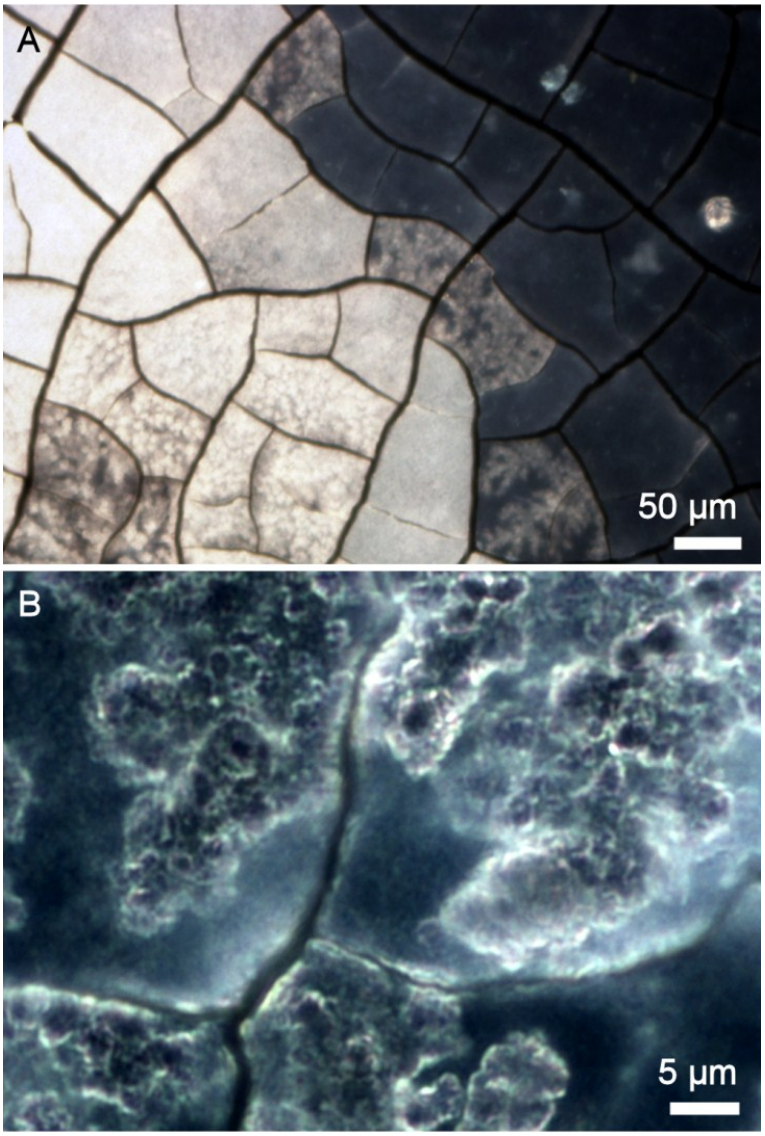

Figure S8: Mineralization of Co^{2+}/ TMV association complexes by salt metathesis. Light microscopy of mineralization products formed by mixing a solution containing metal/virus aggregates with a 100 mM solution of $(NH_4)_2CO_3$ recorded at different magnifications. After being left to sediment for 2 days the precipitate formed in the salt metathesis reaction showed rather unspecific morphologies indicative of an unordered association of mineral nanoparticles and TMV.

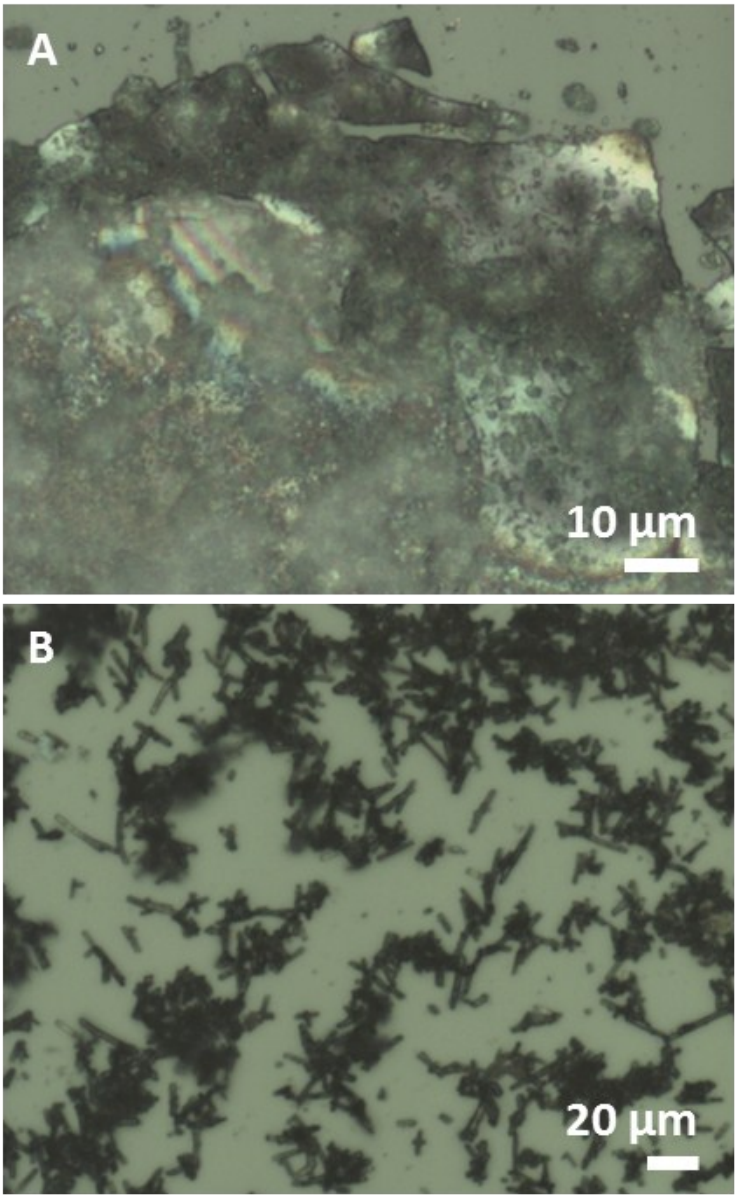

Figure S9. Light microscopy of a precipitate obtained by depositing basic cobalt carbonate from a reactant solution containing concentrations of [Co^{2+}] = 100 mM and [TMV] = 0.02 g·L^{-1}. The isolated solid comprises a mixture of sheet-like structures (A) and microrods (B).

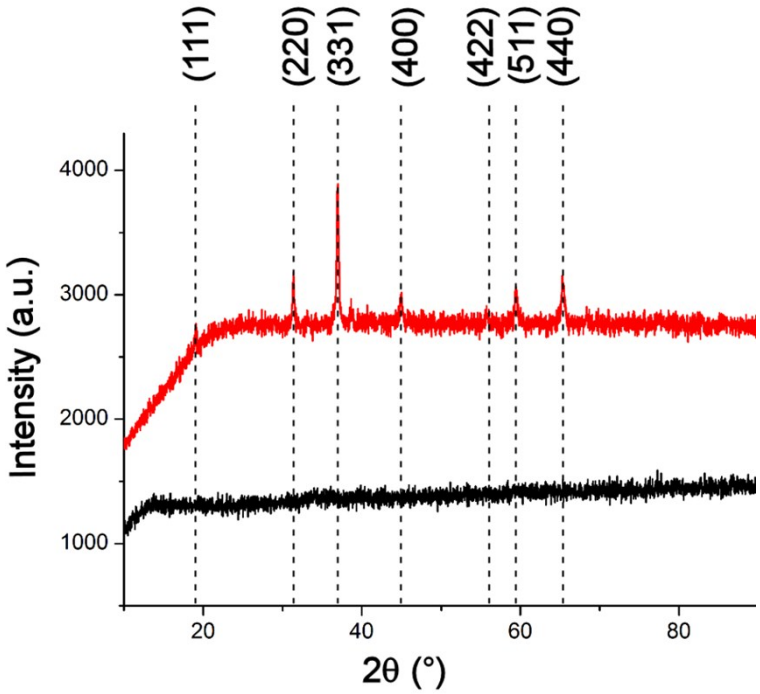

Figure S10. Powder X-ray diffractogram of mineral precipitated from a 100 mM Co(II)-solution in the presence of [TMV] = 0.1 g·L^{-1}. Diffraction data were recorded before (black curve) and after calcination (red curve). The calcined sample shows diffraction peaks in agreement with the spinel-type cobalt oxide structure. In both curves a strong fluorescence background is observed.

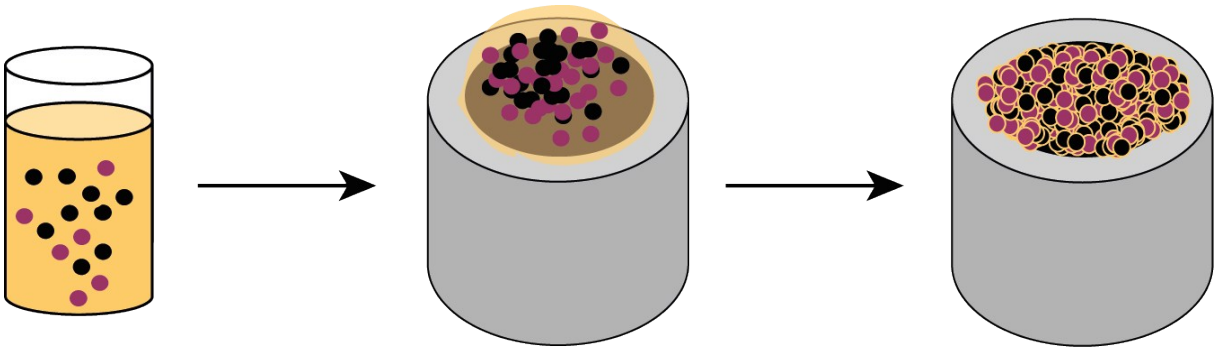

Figure S11: Schematic illustration of the procedure for electrode preparation. Left: GC (purple) and cobalt(II,III) oxide (black) powders are suspended in Nafion solution (yellow). This mixture is then drop-casted onto the GC-RDE electrode (centre). Right: After evaporation of the solvent the solid residue covers the electrode surface.

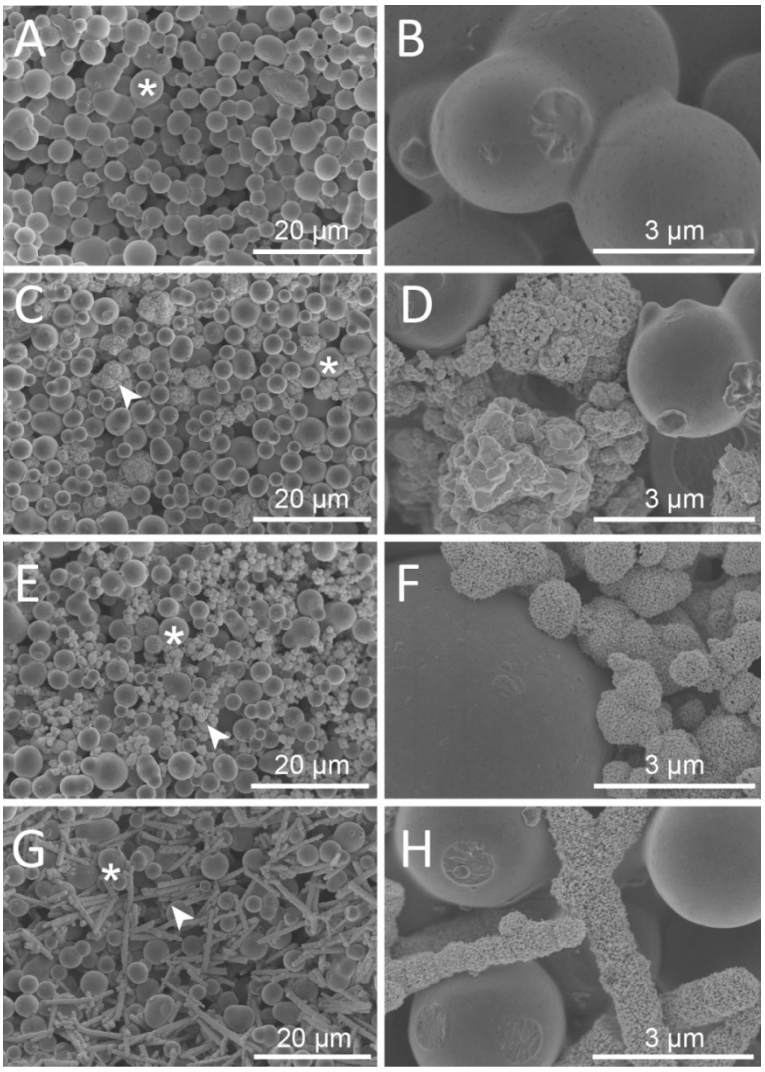

Figure S12. Scanning electron micrographs of electrode surfaces prepared from different Co_3O_4 materials. Overview and detail pictures are presented for electrodes coated with either a pure GC/ Nafion mixture (A, B) or a GC/ Nafion conducting matrix intermixed with commercial Co_3O_4 (C, D) or Co_3O_4 prepared by calcination of carbonate precursors obtained by ammonia diffusion precipitation (E-H). E, F) Bulk material prepared in the absence of additives. G, H) Rods and tubes formed by virus-directed mineralization. In the overview images, GC particles are marked with an asterisk, while the arrowheads point to Co_3O_4 particles.

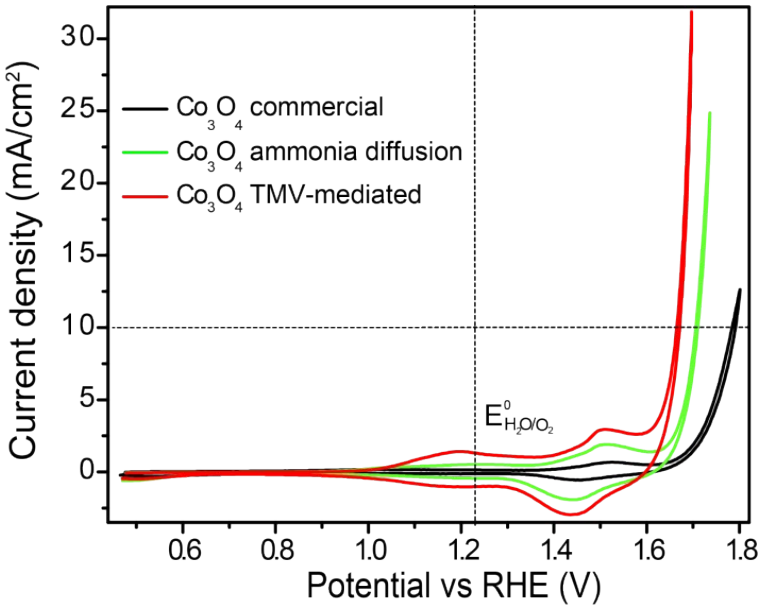

Figure S13. OER performances of different cobalt oxide materials immobilized on electrodes with oxide loadings of 1.4 mg·cm^{-2}. Cyclic voltammograms of Co_3O_4 commercial (black curve), Co_3O_4 ammonia diffusion (green curve) and Co_3O_4 TMV-directed (red curve) at a scan rate of 50 mV·s^{-1} at 2,000 r.p.m. in 0.1 M NaOH. The vertical dashed line marks the $E^0(H_2O/O_2)$, while the horizontal dashed line marks the current density of 10 mA·cm^{-2}, at which the overpotential $\eta_{i=10mA\cdot cm^{-2}}$ is determined. All curves show multiple oxidative waves between 1.1 and 1.5 V vs RHE, which are related to the transitions Co(II)/Co(III) and Co(III)/(IV) of spinel-type cobalt oxide,[4, 5] prior to the onset of the OER.

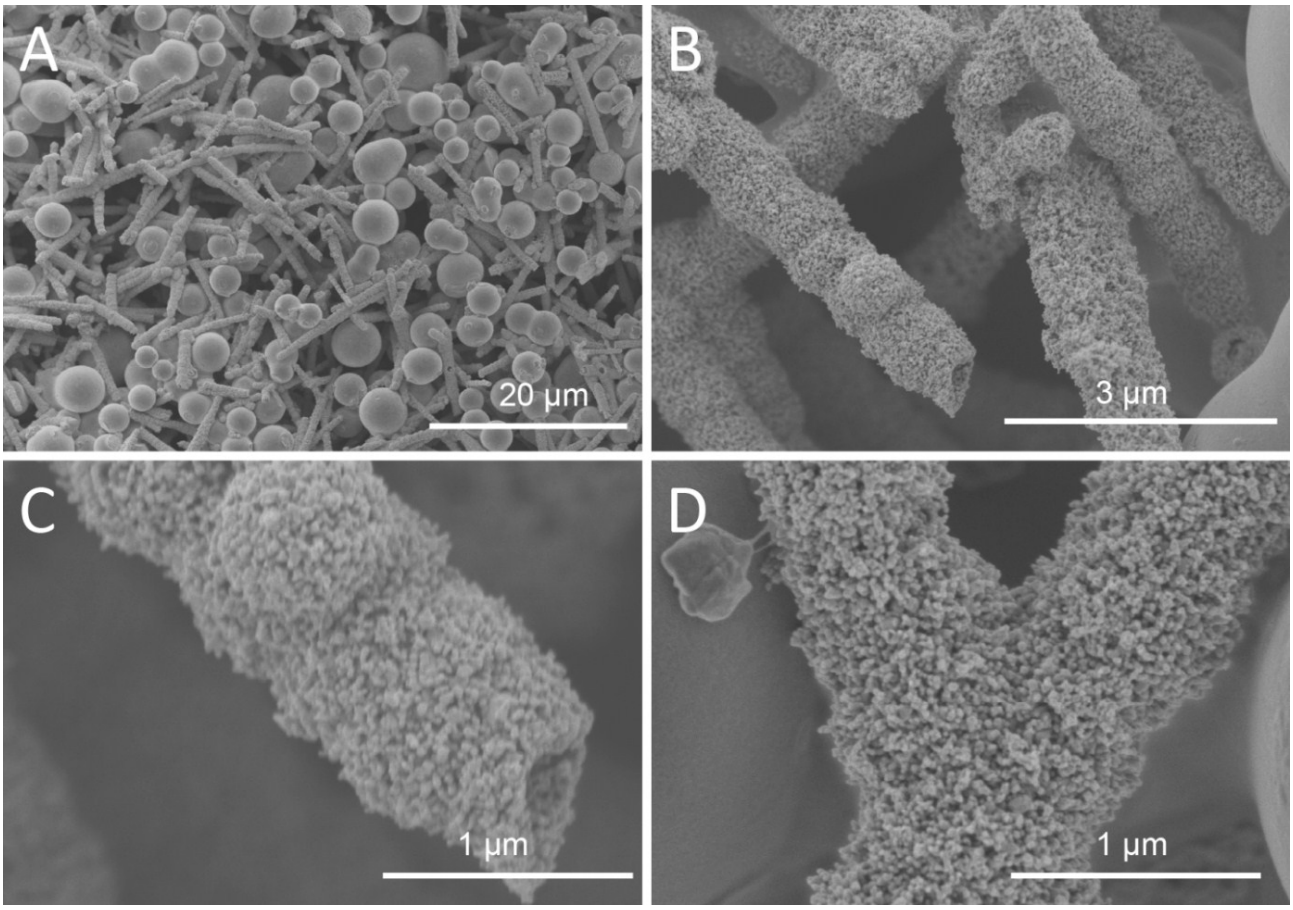

Figure S14. Stability of electrodes fabricated from virus-mediated Co_3O_4 during electrocatalysis. Scanning electron micrographs of an electrode prepared from virus-directed Co_3O_4 recorded after exposure to a current density of 10 $mA \cdot cm^{-2}$ in OER for 10 min (A-C). For comparison, a micrograph of a Co_3O_4 particle on the same electrode before use is shown in (D) at the same magnification as in (C).

3. Chemical Composition of Mineralization Products

A range of analytical techniques including Infra-red and Raman spectroscopies, thermal analysis and powder x-ray diffraction were used to study the chemical composition of the different precipitates before and after calcination. In this section we provide further details on these analyses.

3.1. Mineral Precipitated via Ammonium Carbonate Diffusion in the Absence of Additives.

Upon exposure of a 100 mM solution of $CoCl_2 \cdot 6H_2O$ to ammonium carbonate vapor, a film-like material with blue-green color was first deposited at the air-solution interface after approximately 6 hours. In the progress of the reaction, this interface-grown material slowly changed its color to an intense pink, while light pink mineral particles started to form in bulk after ≈24 hours. Note that these colors are typical for cobalt(II) hydroxide and cobalt(II) carbonate phases as they can be obtained from hydrothermal reactions.

Infra-red (IR) spectra were recorded from dried powders of the earliest interface-grown mineral species as well as the mature precipitate isolated after 48 hours (Fig. S2). Vibration bands characteristic of both, hydroxide and carbonate ligands were identified in the IR spectrum of the final pink precipitate (red line), where this is in agreement with a general composition of $Co(CO_3)_x(OH)_y$. Specifically, the presence of carbonate ions is evidenced by vibration bands at 829 cm^{-1}, 1070 cm^{-1}, and 1391 cm^{-1}, while the peak at 964 cm^{-1} can be assigned to a δ(Co-OH) bending mode.[6] A weak intensity band at 1641 cm^{-1} and a broad band centered at around 3300 cm^{-1} indicate bending and stretching modes of absorbed water molecules, where the shoulder at 3485 cm^{-1} can be assigned to O-H stretching vibrations in the hydroxyl units.[7]

In contrast, the film-like, blue-green product initially deposited at the interface shows comparably weak signals, which points to a more disordered structure at early stages of the reaction. However, a broad absorption band at 829 cm^{-1}, which is characteristic of the symmetric bending mode of carbonate ions (ν_2 (CO_3^{2-})), can be clearly identified. The band at 3485 cm^{-1}, which is related to stretching vibrations of the hydroxyl groups, was found to be very sharp and pronounced in the early stage sample. The band attributable to the asymmetric stretching mode of the carbonate ions, which occurs at around 1400 cm^{-1} in the mature material, is split into two components in the spectrum recorded from the early stage precipitate, indicating the presence of two non-equivalent types of carbonate ions. This might be an additional indication for a less ordered or even amorphous nature of the film-like material extracted after 6 hours.

The mature precipitate was further investigated by thermal analysis and powder x-ray diffraction. Thermogravimetric analysis (Fig. S2) revealed a first weight loss event in the temperature range between 80°C and 165°C, where this can be attributed to a gradual release of surface-bound and structural water. A sharp peak appeared in the DSC profile at 227.5°C indicating an exothermal event. Additionally, a further weight loss of 19.4 wt.-% is recorded in the temperature range between 165°C and 350°C. This observation can be explained by the simultaneous elimination of CO_2 and H_2O during the chemical transformation from $Co(CO_3)_x(OH)_y$ to spinel-Co_3O_4 in air atmosphere.[8] Assuming that the first weight loss event observed in the thermogram, which amounts for 8 wt.-% of the total mass of the investigated specimen, was entirely due to the evaporation of water, we calculate that the solid mineral residue left at 165°C has lost 21% of its original weight during the transformation into Co_3O_4, where this value is smaller than the theoretical weight loss of pure $CoCO_3$ (32.5%), but higher than the weight loss expected for the stoichiometric hydroxide $Co(OH)_2$ (13.6%). Hence, the results of the thermal analysis are in agreement with a precursor composition including both, carbonate and hydroxide anions ($Co(CO_3)_x(OH)_y$).

With the aim to exactly determine the crystallographic phase of the mineral precursor, x-ray diffraction was performed on a powder sample (Fig. S3, black line). Due to a strong fluorescence background presumably originating from the interaction of Cu-K_α radiation with the cobalt-containing sample, it was not possible to identify and assign any distinct Bragg reflections attributable to the basic carbonate precursor. After thermal conversion of the precursor at 400°C, however, the diffractogram clearly showed a peak profile characteristic of Co_3O_4.[9]

3.2. Virus-Directed Mineralization.

Vibrational spectroscopy and thermal analysis were performed to study the composition of a mineralization product precipitated *via* ammonium carbonate diffusion from a solution with reactant concentrations of $[Co^{2+}]$ = 100 mM and [TMV] = 0.1 g·L^{-1}. The infra-red spectrum recorded for a material recovered from the reactant solution after 2 days (Fig. 4C) was largely similar to that of the purely inorganic basic cobalt carbonate showing exclusively bands attributable to carbonate and hydroxyl units as well as a broad signal centered at around 3250 cm^{-1}, where the latter is indicative of adsorbed or structural water molecules. This suggests that co-precipitation with the biogenic nanoparticles did not substantially affect the composition of the inorganic phase.

In complementation of the IR-measurements, Raman spectroscopy was performed on selected particles and particle aggregates (Fig. 5A). These measurements confirmed that the purely inorganic material (black curve in Fig. 5A) and the mineral phase deposited in the presence of TMV particles (grey curve in Fig. 5A) were similar in their composition showing vibration bands that can be assigned to

CO_3^{2-} and Co-O modes. Specifically, characteristic vibration bands appeared at Raman shifts of 453 cm^{-1}, 534 cm^{-1}, 752 cm^{-1}, and 1085 cm^{-1}.[7] The sample prepared in the absence of TMV additionally showed three weak bands at 482 cm^{-1}, 621 cm^{-1} and 690 cm^{-1}. As these signals appear in spectral regions characteristic of the Co-O vibrations in Co_3O_4, they might originate from partial oxidation of the product during illumination with the Raman laser even after very short illumination times. After calcination at 400°C, the Raman spectrum of the TMV-mediated material exclusively showed vibration bands attributable to Co_3O_4, which were identified at 191 cm^{-1} (F_{2g}), 473 cm^{-1} (E_g), 513 cm^{-1} (F_{2g}), 611 cm^{-1} (F_{2g}), and 679 cm^{-1} (A_{1g}).[10]

Similarly, only very subtle differences were observed between the TGA and DSC profiles of $Co(CO_3)_x(OH)_y$ deposited in the absence (Fig. S2) or presence of TMV (Fig. S6). Most importantly, the transformation temperatures for the precursor-to-oxide transition were the same for both precipitates (Figs. S2 and S6). In this context, the temperature required for decomposition of the basic cobalt carbonate and formation of the spinel-Co_3O_4 crystal lattice critically depends on the crystallinity of the precursor phase. The weight loss recorded in the temperature range between RT and 200°C was, however, slightly increased from 8 wt.-% (additive-free sample) to 9.6 wt.-%, when tobacco mosaic viruses had been added to the reactant solution and a small shoulder appeared in the DSC curve at a temperature of ~175°C (Fig. S6, red arrow). In order to study the origin of the shoulder observed in the composite material, we performed thermal analysis on a suspension of non-mineralized TMV in water. This experiment, however, did not confirm a thermal event in the bare virus occurring at the specified temperature.

Given that TGA analysis did not provide any indication for a partial decomposition of the biogenic nanorods at temperatures < 200°C (Fig. S6), we speculate that the higher overall weight loss in the virus/ mineral composite sample as compared to the purely inorganic basic cobalt carbonate originates from an increased incorporation of water molecules into the mineralized product due to association with the hydrophilic virus particles. In this, we emphasize, however, that the TGA-profile of the bare virus at very low temperatures (T < 100°C) is strongly dominated by the evaporation of excess water from the virus particle suspension, which could potentially mask transformations in the protein-based biotemplates.

After calcination of the virus/ mineral composite, the x-ray diffraction profile showed the characteristic (111), (220), (331), (400), (422), (511), and (440) Bragg diffraction peaks of spinel-type Co_3O_4,[9] which demonstrates that this catalytically active transition metal oxide phase can be obtained by thermal conversion of the virus-directed material. In similarity with the sample precipitated in the absence of virus particles, however, the diffractogram of the TMV/ mineral precursor recorded prior

thermal conversion was dominated by a strong fluorescence background that did not allow us to discern any sample-related diffraction peaks for phase identification.

References

1. S. N. Chapman, *Methods in Molecular Biology*, 1998, **81**, 123-129.
2. J. Sambrook and D. W. Russell, *Molecular Cloning. A Laboratory Manual. 3 ed*, Cold Spring Harbor Laboratory Press New York, 2001.
3. D. T. Sawyer, A. Sobkowiak and J. L. Roberts, *Electrochemistry for Chemists*, John Wiley & Sons New York, 1995.
4. E. B. Castro, C. A. Gervasi and J. R. Vilche, *Journal of Applied Electrochemistry*, 1998, **28**, 835-841.
5. P. Nkeng, G. Poillerat, J. F. Koenig, P. Chartier, B. Lefez, J. Lopitaux and M. Lenglet, *Journal of The Electrochemical Society*, 1995, **142**, 1777-1783.
6. R. Yu, P. Tao, X. Zhou and Y. Fang, *Journal of Alloys and Compounds*, 2008, **461**, 574-578.
7. J. Yang, H. Cheng and R. L. Frost, *Spectrochimica Acta Part A: Molecular and Biomolecular Spectroscopy*, 2011, **78**, 420-428.
8. L. Avramov and C. Betschev, *Zeitschrift für Anorganische und Allgemeine Chemie* 1971, **383**, 96-102.
9. X. Liu and C. T. Prewitt, *Physics and Chemistry of Minerals*, 1990, **17**, 168-172.
10. V. G. Hadjiev, M. N. Iliev and I. V. Vergilov, *Journal of Physics C: Solid State Physics*, 1988, **21**, L199.